Australas Phys Eng Sci Med (2014) 37:393–403
DOI 10.1007/s13246-014-0273-x

SCIENTIFIC PAPER

Computer-assisted segmentation of CT images by statistical region merging for the production of voxel models of anatomy for CT dosimetry

M. Caon · J. Sedlář · M. Bajger · G. Lee

Received: 16 December 2013 / Accepted: 11 April 2014 / Published online: 26 April 2014

Abstract The segmentation of CT images to produce a computational model of anatomy is a time-consuming and laborious process. Here we report a time saving semi-automatic approach. The image-processing technique known as "statistical region merging" (SRM) was used to pre-segment the 54 original CT images of the ADELAIDE data set into regions of related pixels. These regions were amalgamated into organs and tissues by a program operated through a graphical user interface. This combination of SRM and GUI was used to build a voxel computational model of anatomy. The "new" version of ADELAIDE was compared to the "old" version by simulating an abdominal CT procedure on both models and comparing the Monte Carlo calculated organ doses. Seventeen of the 21 SRM–GUI segmented tissues received doses that were within 18 % of the doses received by the manually segmented tissues. Hence the SRM–GUI segmentation technique can produce a computational model that is not functionally different from a manually segmented computational model. The SRM–GUI segmentation technique is able to reduce the time taken to construct a voxel tomographic model from CT images.

Keywords Voxel model · Image segmentation · Statistical region merging · CT dosimetry

M. Caon (✉) · J. Sedlář · M. Bajger · G. Lee
Medical Devices Research Institute, Flinders University, Bedford Park, SA, Australia
e-mail: Martin.Caon@flinders.edu.au

M. Caon
School of Health Sciences, Flinders University, Bedford Park, SA, Australia

J. Sedlář · M. Bajger · G. Lee
School of Computer Science, Engineering and Mathematics, Flinders University, Bedford Park, SA, Australia

J. Sedlář
Institute of Information Theory and Automation, Academy of Sciences of the Czech Republic, Prague 1, Czech Republic

Introduction

Medical image segmentation is the process of identifying where the boundary of a tissue or organ lies, drawing it and then labeling the pixels of that tissue with one common greyscale value, different from the values assigned to the other identified tissues. The task is undertaken in order to construct realistic whole body models of human anatomy which can be used (for example) to calculate absorbed dose to organs and tissues from computed tomography (CT) procedures. The manual segmentation process is very time consuming both because of the time required to identify and draw contours around all of the tissues in a single tomographic image, and because of the large number (300–600) of individual images that are required to span the head to foot anatomy of an individual at (say) 3 mm intervals. Consequently there have been efforts to speed the process by semi-automating it.

The segmentation of CT images can be said to have started in 1984 when Gibbs et al. [1], in order to determine dose from dental radiography by computer Monte Carlo simulation, imaged the head and trunk of a female cadaver and segmented the pixels as air, lung, fat, muscle, bone or tooth. No details of the segmentation are provided, however it can be safely assumed that the 64×64 image arrays were processed manually. Veit et al. [2] were the first to describe the segmentation of an entire body set of tomographic images. However their description of the segmentation of

BABY (142 slices) and CHILD (144 slices) was brief, and consisted of stating that while skin and skeleton could be segmented automatically, all other organs were segmented manually and one slice at a time.

Zubal et al. [3] developed an in-house program to display CT images and permit medical staff to outline the more than 3,000 contours required to characterise the organ boundaries. Each organ outline was filled with a unique integer index value using a region-of-interest colouring routine.

Magnetic resonance images of anatomy are another source of anatomical information and were used by Dimbylow [4] and Jones [5] to construct a computational model modified to match the size of Reference Man—the model is known as NORMAN. In this case, greyscale images were segmented "semi-automatically" using thresholding. Where this was not possible, anatomical texts were used for guidance and tissue was manually drawn into the image. Where necessary, for example with bone, images were edited by hand and this proved to be a challenge.

The 54 slice torso model ADELAIDE was segmented manually using the commercial software *PaintShop Pro* and *Image-Pro Plus* slice by slice. Contours were hand drawn and pixel values coloured in using the "flood-fill" facility and, where necessary, by hand pixel by pixel [6].

Xu et al. [7] used colour photographs of anatomy from the physically sectioned cadaver of the Visible Human Project to construct VIP-Man. The images had already been segmented "mostly by manual procedures" but Xu et al. segmented some other selected tissues by automatic and manual image processing means based on colour. This was possible as the images were colour photographs rather than reconstructed medical images in a grey scale.

Zankl and Wittmann [8] used dedicated image processing commercial hardware and software (called MIPRON) to segment "Golem" without manually drawing organ boundaries. They avoided manual drawing by developing a series of macros that used thresholding and morphological operations (such as dilation, erosion, filling etc.) into an algorithm. It is not clear from the otherwise detailed description given, how much supervision was required by the operator. Saito et al also used MIPRON (as well as Visilog) to segment the 170 (or so) CT images of the Japanese computational model known as "Otoko" [9]. They also used thresholding and morphological image-processing techniques on a slice by slice basis.

Rather than using commercially available image processing software, Nipper et al. [10] wrote their own image processing code using IDL (Interactive Data Language) which they have called *CT_Contours*. *CT_Contours* enabled the drawing of contours by using image-processing techniques such as: basic thresholding, pixel growing, voxel growing, region growing and by manual segmentation. A region of interest (a tissue to be segmented) could be created in the transverse, coronal or sagittal planes. The results of automatic segmentation were supervised so that errors could be corrected by manual drawing.

Nagaoka et al constructed models of a Japanese male and female from MRI images. They wrote: "It is impossible to divide the voxels in the original images into corresponding tissues or organs automatically with sufficient accuracy using presently available image-processing technologies" [11]. Consequently, tissue and organ-identification was performed manually on individual images by medical staff operating software on personal computers. There were more than 800 images for each model and the task took longer than 3 years. While the identification of tissue boundaries is necessarily somewhat subjective, the work, when done by experts can be considered best practice.

Kramer et al constructed their adult female computational model FAX from the torso of a 37 year-old, the legs and feet of a 62 year-old and the scaled head and arms of the male MAX model [12]. The 357 images were segmented manually using *Microsoft PAINT* to colour each organ and tissue of interest.

Lee et al. also used the University of Florida developed in-house software *CT_Contours* to identify and contour images on a slice by slice basis for five head and torso paediatric models. The software allowed thresholding, edge detection, dilation along with manual drawing and modification [13]. For some tissues with insufficient contrast to make them distinguishable in the images, an informed decision as to their shape location had to be made, and these decisions were reviewed by an experienced paediatric radiologist.

In the Chinese equivalent of the Visible Human Project, colour photographic images of sectioned male and female cadavers were manually segmented with *Adobe Photoshop* software to produce the Chinese adult male voxel phantom CNMAN [14] and the voxel-based Chinese reference female phantom (VCRP-woman) [15] respectively. The tissues in the images were identified visually and their borders outlined and filled with a colour to aid their visualisation. Red bone marrow in the male was distinguished from yellow bone marrow using colour thresholding.

A voxel model of a Korean male cadaver was produced similarly. The 33 year old leukemia victim was adjusted from a height of 164 to 171 cm and is known as HDRK-man [16]. Kim et al. found that the colour images were better than grey-scale CT or MR images for segmentation purposes because the color images made different tissues that were not clearly visible with CT or MRI, distinguishable. Eleven tissues in the images used for HDRK-man had already been segmented by Park et al. [17] who used the "magnetic lasso" tool of *Adobe Photoshop* to

semi-automatically draw the contours for these tissues which were then coloured in. Kim et al. used the same software and tool to "automatically" segment eight additional tissues. That is, by using this image-processing tool, the region that surrounds a pixel manually selected by a mouse click, and whose pixels are sufficiently close in colour to the selected pixel, is automatically identified and enclosed with a contour. The other organs were segmented manually, again using the lasso tool in *Adobe Photoshop* which Kim et al state: "significantly expedited the segmentation process".

The art of image segmentation for the purpose of constructing a computational anatomical model of the whole human body that can be used for radiation dosimetry, has not progressed far over the 25 years it has been practiced. It began as a time-consuming manual process and remains today a largely manual process, albeit with varying degrees of semi-automation. Using automated methods to reduce the time required to produce a voxel model of anatomy from many months to a few days or weeks remains an elusive goal.

Our approach to automating the image segmentation process is to use the technique of statistical region merging (SRM) [18] to identify regions of adjoining pixels that possibly belong to the same tissue [19]. The SRM technique has proved to be a great tool for producing efficient and usable segmentations for analysis of natural scene images (see also e.g. [20]). In medical applications, Celebi et al. [21, 22] applied the technique for border detection in dermoscopy images to help with skin cancer detection. Bajger et al. [23] successfully applied the SRM technique to mammograms for breast cancer detection. Lee et al. [19, 24, 25] applied SRM for segmenting CT images, while Wong et al. [26] used SRM for prostate lesion segmentation in MRI images. The above shows that SRM-based techniques can be successfully applied to a range of challenging tasks in medical image segmentation.

The segmentation of a tissue or organ is completed when adjacent regions are selected by the user as belonging to the one tissue and amalgamated. The first step of applying SRM to medical images is achieved rapidly (in about 1 s) by a computer algorithm. The second step is achieved by using a graphical user interface (GUI) that we have developed for the purpose. This article reports on the usefulness of the combination of SRM and GUI in segmenting medical images for the purpose of constructing voxel models of anatomy which can be used for dosimetry purposes. It compares a voxel model of anatomy produced by manual segmentation of CT images (that is, the ADELAIDE model [6]), with a version of the voxel model produced by using SRM and our GUI applied to the same CT data set. The comparison is made by comparing the number of voxels assigned to each tissue and the absorbed dose to organs of the two voxel models when both are subjected to the same Monte Carlo (MC) simulated CT imaging procedure.

Our goal is to determine whether a voxel model of anatomy that is produced in a short time by the method above, can be used to calculate tissue and organ doses from a CT procedure, that are comparable to those achieved when a manually segmented voxel model is used.

Methods

Pre-segmentation using statistical region merging

SRM segmentation is a bottom-up process of combining image pixels into bigger regions based on the following criterion. The two regions R_1 and R_2 are merged into a single region if the difference between average intensities across these regions does not exceed the value

$$g\sqrt{\frac{\ln(2/\sigma)}{2Q}\left(\frac{1}{\#R_1}+\frac{1}{\#R_2}\right)},$$

where $g = 256$, the number of grey level values, $\#R$ is the number of pixels in the region R, σ is a very small number inversely proportional to the square of number of pixels in the image I, for example, $\sigma = \frac{1}{6(\#I)^2}$, and Q is a parameter whose value has to be set by the user for an image at hand. Note that Q value is the only parameter which needs to be determined by the user. In practice, it is not difficult to choose values of Q which result in satisfactory segmentations for a large range of images.

The Q value quantifies statistical complexity of the image. Thus, the value of Q is responsible for the coarseness of the segmentation. In this study, a low Q value often results in under-segmentation, that is, not enough regions are identifed to distinguish different organs sufficiently. A high Q value, on the other hand, often results in over-segmentation, that is, too many regions are identified within one tissue. In the latter case, amalgamating the regions becomes necessary. Bajger et al. [23] showed that in some applications it may be possible to develop an analytical criterion for an estimation of Q value resulting in the required coarseness of the segmentation.

It is worth pointing out that our choice of SRM over other well-known and widely used segmentation methods such as the Mean-Shift [27] or the Normalized Cut [28] was motivated by the computational efficiency of the SRM algorithm and its successful previous applications to medical image analysis, as mentioned above. Our GUI framework can readily work with any pre-segmented images regardless of the method used to produce the segmentation.

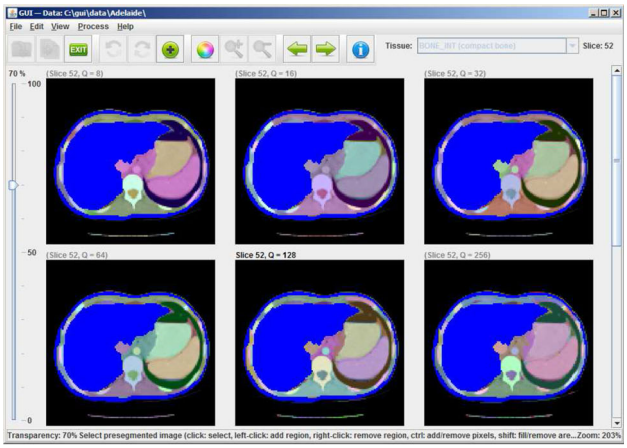

(a)

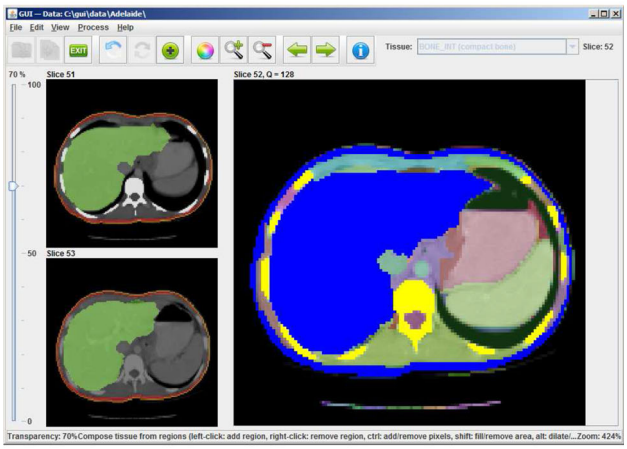

(b)

Fig. 1 GUI screenshots: **a** slice 52 displayed for six Q values and showing skin, sub-cutaneous fat and liver in *blue*, indicating that those pixels are protected from being reassigned to another tissue; **b** slice 52 with Q value 128 selected for amalgamating regions of bone (and enlarged to facilitate the process). Amalgamated regions are shown in *yellow*. At *left* are displayed the two adjacent slices

Description of the graphical user interface

We use the SRM technique to pre-segment the pixels of CT images into regions. The GUI is then used to amalgamate regions into the shapes of organs or tissues. The GUI uses medical (CT)images and their corresponding SRM pre-segmented images as input and saves images of tissue shapes segmented by the user from the pre-segmented images. Thus the GUI is not used for image processing, as the SRM technique processes the CT images to pre-segment them. An external program generates a set of SRM pre-segmented images from each CT image. For the present work, for example, we generated 64 different SRM images from each CT image, but chose to use only the values $Q = 8, 16, 32, 64, 128, 256$ and 512.

The GUI displays a pre-defined number (a default of six) of consecutive CT images on the screen at one time. SRM pre-segmented images with regions identified by different colours are overlaid on the original greyscale CT images. The GUI allows the user to adjust the transparency so that amalgamated SRM regions can be compared to the tissues they represent. The GUI user works with one tissue at a time from those available in a drop down list. The tissue names and number of tissues may be adjusted by the user and are independent of the SRM pre-segmentation. After selecting a tissue the user selects the first and last slice of the stack of consecutive slices to work on. The GUI then displays a predefined number (default six) of images of the first slice at different Q values—again overlaid on the original CT greyscale images so that the correspondence between SRM regions and tissue boundaries can be viewed by changing the transparency. The user chooses the Q value most appropriate for segmenting the tissue and that image may be magnified for convenience. Having images with a range of Q values is useful as it is common for different Q values to be used for different tissues and even for the same tissue in a different slice.

The user clicks on SRM regions to select (or deselect) them for amalgamation into a single region. Selection colours the region yellow so that the amalgamated shape is seen (see Fig. 1). When satisfied with the shape, the user proceeds to the next slice. The GUI is not primarily an image processor but has some image processing capabilities which are useful in cases where the tissue shape cannot be adequately composed of the available SRM regions. The available image processing methods in the GUI that may be applied to the SRM images to adjust the segmented shape include adding or removing pixels, boundary smoothing, morphological dilation and erosion, filling in holes and labeling of all remaining unlabeled pixels. Regions and pixels that have already been assigned to a tissue are indicated by a blue overlay (see Fig. 1) and are prevented from being reassigned to a subsequent tissue (except if the user specifically chooses to). In this way it is clear which regions of the image remain to be segmented.

The GUI is written in the Java programming language so is portable between computers. Since the GUI operates on pre-segmented regions rather than on a pixel level, the segmentation is much faster than pixel-level segmentation. To segment a tissue shape, the user typically amalgamates a limited number of SRM regions. For large organs, such as liver or spleen, the number of regions may be two to four. The organ boundaries achieved by using the GUI to amalgamate pre-segmented SRM regions are not as smooth as those achieved by manually drawing the boundaries (even after applying smoothing), however the process is much faster.

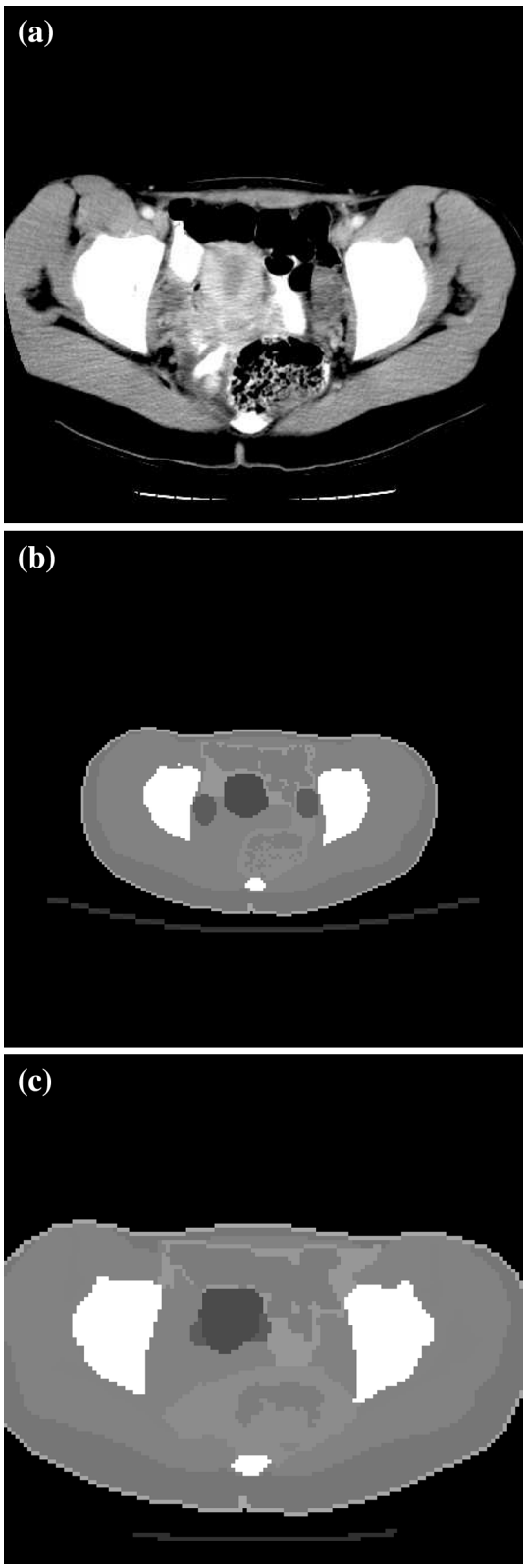

Fig. 2 Image 84 showing truncation of the lateral parts of the hips due to the restricted field of view **a** an original CT data, **b** original manual segmentation, **c** the SRM–GUI segmented image

Experiment

Data set

The original clinical CT data from which ADELAIDE was constructed were 54 images (at 1 cm intervals) of the torso at 451 × 451 pixels, that were acquired in 1996 before the DICOM image standard had been adopted [6]. For the original manual segmentation, these images were resized to 128 × 126 pixels because of the limited memory available in desktop computers of the time. The 29 cm diameter field of view truncated some superficial anatomy in the superior 16 and inferior 13 slices (see Fig. 2 for an example). For these slices, this missing anatomy (skin, sub-cutaneous fat and muscle at the shoulders and hips) was at the time, added by hand for the manually segmented ADELAIDE. This addition had the effect of extending the lateral dimension of the manually segmented ADELAIDE from 128 to 140 pixels (in the worst case).

Voxel model produced by GUI

In order to compare the GUI segmentation with manual segmentation, the SRM algorithm needs to work with the original ADELAIDE CT images (albeit resized to 128 × 126 pixels), so was applied to the truncated images described above. This was deemed to be acceptable as: a) this was the clinical data available to us, and b) comparing calculated organ doses to an SRM segmented model built from truncated images, to organ doses calculated to a manually segmented ADELAIDE for entire anatomy, would be a more searching test of the ability of the SRM–GUI technique to deliver accurate segmentation.

The SRM technique is in theory able to segment thin structures such as the skin, provided that the skin's image is present and uncorrupted in the image. However it would produce a great many very small regions which would be time-consuming to amalgamate. So for this work, the external boundary of the manually segmented ADELAIDE was used to form the skin (of one pixel thickness) of the SRM–GUI version.

Differences between manual Adelaide and SRM–GUI Adelaide

Cortical bone and its overlying one pixel thick bone surface were segmented separately in the manually segmented ADELAIDE but bone surface and bone were not distinguishable in the SRM–GUI version. So to compare the two versions of ADELAIDE, bone and bone surface are combined in Table 1 and the doses averaged using the formula:

Table 1 Organ doses to the manually segmented and SRM–GUI segmented versions of the ADELAIDE voxel model, with uncertainties in brackets

Organ/tissue	Organ dose (nGy cm^2) for manual seg.	Organ dose (nGy cm^2) for SRM–GUI seg.	Percentage difference (GUI/manual)
Bone	4.56 (±0.06 %)	9.34 (±0.04 %)	
Bone surface	21.61 (±0.06 %)	na	
Combined bone and bone surface	10.74	9.34 (±0.04 %)	−13
Heart	1.80 (±0.13 %)	2.06 (±0.18 %)	14
Spinal cord	1.60 (±0.78 %)	2.11 (±0.60 %)	32
Skin	13.8 (±0.06 %)	14.67 (± 0.06 %)	7
Sub cut fat	9.33 (±0.03 %)	9.64 (±0.04 %)	3
Muscle	5.03 (±0.02 %)	5.64 (±0.03 %)	
	Including soft tissue		
Soft tissue	na	2.37 (±0.17 %)	
Combined muscle and soft tissue	5.03 (±0.02 %)	5.24	4
Breasts	1.10 (±0.38 %)	1.25 (±0.35 %)	14
Lungs	3.89 (±0.15 %)	4.78 (±0.07 %)	23
Oesophagus	1.67 (±0.80 %)	1.93 (±0.78 %)	15
Kidneys	8.00 (±0.15 %)	9.02 (±0.17 %)	13
Liver	5.41 (±0.08 %)	6.39 (±0.06 %)	18
Spleen	15.55 (±0.13 %)	17.23 (±0.13 %)	11
Stomach	3.55 (±0.18 %)	4.05 (±0.19 %)	14
Small bowel (wall and contents)	2.27 (±0.12 %)	1.50 (±0.20 %)	
(wall and contents)	Including tra+asc colon		
Large bowel	5.31 (±0.17 %)	3.67 (±0.13 %)	
	des+rec	asc+tra+des+rec	
Combined small and large bowel {including gas}	3.07	3.03	−1
Pancreas	1.90 (±0.76 %)	2.14 (±0.81 %)	13
Gall bladder	2.88 (±1.95 %)	2.98 (±0.76 %)	3
Uterus	0.24 (±1.40 %)	0.31 (±2.09 %)	25
Ovaries	0.32 (±5.51 %)	0.31 (±5.82 %)	−3
Bladder	0.17 (±2.28 %)	0.21 (±2.26 %)	18
Thymus	1.28 (±1.69 %)	0.94 (±1.15 %)	−27
Trachea	0.62 (±3.38 %)	1.07 (±1.62 %)	71
Thyroid	0.53 (±1.56 %)	0.43 (±2.02 %)	−18

$$[(P_b \times D) + (P_{bs} \times D)]/(P_b + P_{bs})$$

where D stands for the dose, P_b indicates number of bone pixels, and P_{bs} is the number of bone surface pixels.

The SRM–GUI segmentation of ADELAIDE includes the ascending, transverse, descending, sigmoid colon and rectum as one tissue (colon, including the contents), whereas in manually segmented ADELAIDE colon did not include the upper large intestine. At the time ADELAIDE was segmented manually, ICRP60 included the upper large intestine as a remainder tissue. Furthermore, upper large intestine was not distinguished from small intestine in manual ADELAIDE. So to compare the two versions of ADELAIDE, small and large intestine are combined and doses averaged in Table 1. Gas within the bowel was segmented in both versions. In GUI-SRM segmented ADELAIDE, soft tissue that was not muscle or sub-cutaneous fat was segmented separately. However in manual ADELAIDE, such soft tissue was assigned to fat or muscle. Again for comparison purposes, muscle and soft tissue are combined and doses averaged in Table 1.

Monte Carlo simulation

A user code that interfaces with the Monte Carlo code EGSnrc [29] was used to simulate a CT examination of the abdomen (from the top of the liver to top of the pelvis). EGSnrc was used with low energy photon options

(Rayleigh scattering, electron impact ionisation and bound Compton scattering) selected. A 120 kV spectrum with 4.9 mm Al (equivalent) filtration was used and attenuated through a "bowtie" beam-shaping filter. The simulated photons spread from a point source into a fan beam of width 1 cm at the isocentre (in the absence of the anatomy) and circled the anatomy without amplitude modulation. An abdomen examination was chosen for the simulation rather than a chest or pelvic examination as the CT images from which ADELAIDE was constructed have parts of the shoulders and hips truncated by the radius of the field of view. The truncated anatomy was drawn in by hand when ADELAIDE was manually segmented, but is absent from the SRM–GUI segmented version of ADELAIDE prepared for this work. An input file was produced for each of the manually segmented ADELAIDE and the SRM–GUI segmented version. They differed only in the assignation of tissues to voxels.

The Monte Carlo simulation was run for 3.7×10^8 histories per slice (this was enough to produce a photon flux of 1.0×10^7 photons/cm^2 at the scanner isocentre in the absence of the phantom). Un-normalised absorbed doses to the organs/tissues of the manually segmented ADELAIDE and to the SRM–GUI segmented version of ADELAIDE were calculated in order to determine whether the differences between the segmented anatomies were sufficient to produce large differences in organ doses.

Results

Figure 3 shows the effect of using different Q values for pre-segmenting images by using SRM. Note that for higher Q values, pre-segmented regions are smaller. For example the heart is segmented as a single region when $Q = 16$, but as several regions when $Q = 64$ or 256. Note also that different regions of the same tissue (e.g. bone) are identified as different SRM regions and so given a different colour. Figure 4 shows two examples of a CT image (451×451 pixels) from the ADELAIDE data set, its original manual segmentation (from a 200×200 pixel image) and the SRM–GUI segmentation (from the same image but at 128×126 pixels). Table 1 lists 21 organs or tissues (or organ groups) segmented in ADELAIDE along with the un-normalised Monte Carlo calculated absorbed dose to the tissue, while Table 2 lists the number of voxels assigned to each tissue. Column two displays the data for the manually segmented original ADELAIDE, while column three lists the data for the SRM–GUI segmented ADELAIDE. In the fourth column are shown the percentage differences between the Monte Carlo calculated organ doses or between the numbers of voxels in the two versions of

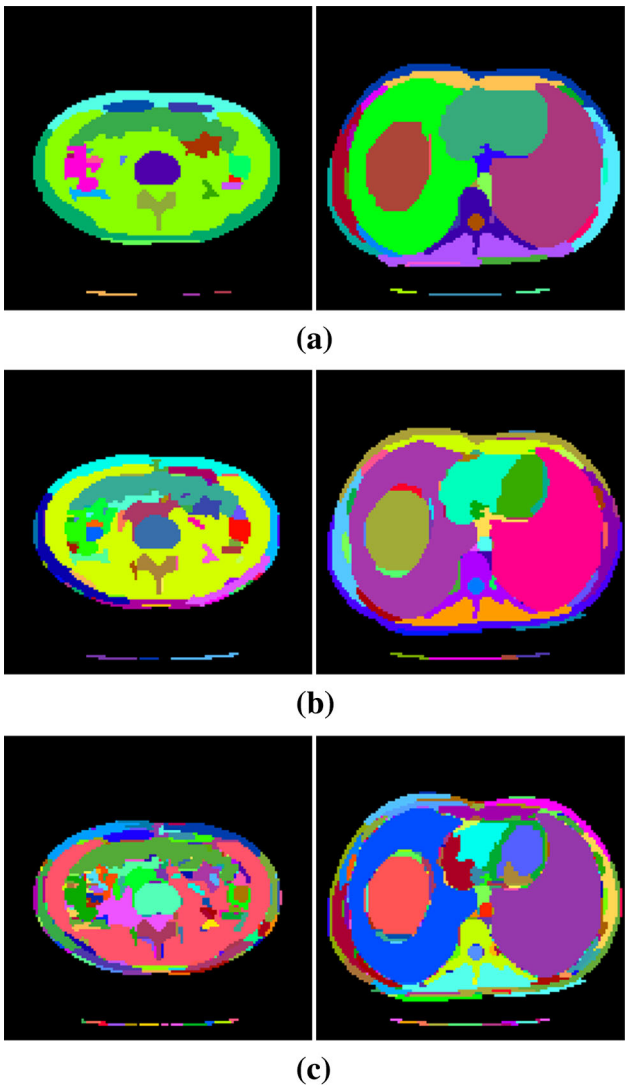

Fig. 3 CT images 68 (*left*) and 48 (*right*) pre-segmented into regions (of *different colour*) by the SRM technique with different Q values: **a** $Q = 16$, **b** $Q = 64$, **c** $Q = 256$

ADELAIDE. Seventeen of the 21 pairs of organ doses are within 18 % of each other.

When numbers of voxels segmented to each tissue are compared, liver, bone, kidney, heart, breasts, skin, combined muscle and soft tissue, and combined small and large intestine (including contents) differed by 0.5, 1, 2, 4, 7, 8, 10 and 10 percent respectively. Thirteen of the 21 SRM–GUI segmented tissues are within 18 % of the manually segmented values. A further four are small organs or tissues (pancreas, ovaries, thymus and thyroid) that were not amenable to SRM pre-segmentation and required manual segmentation with the GUI. The greatest percentage differences were for trachea and gall bladder (and contents). These tissues (as well as ovaries) have the smallest numbers of voxels in manually segmented ADELAIDE so the

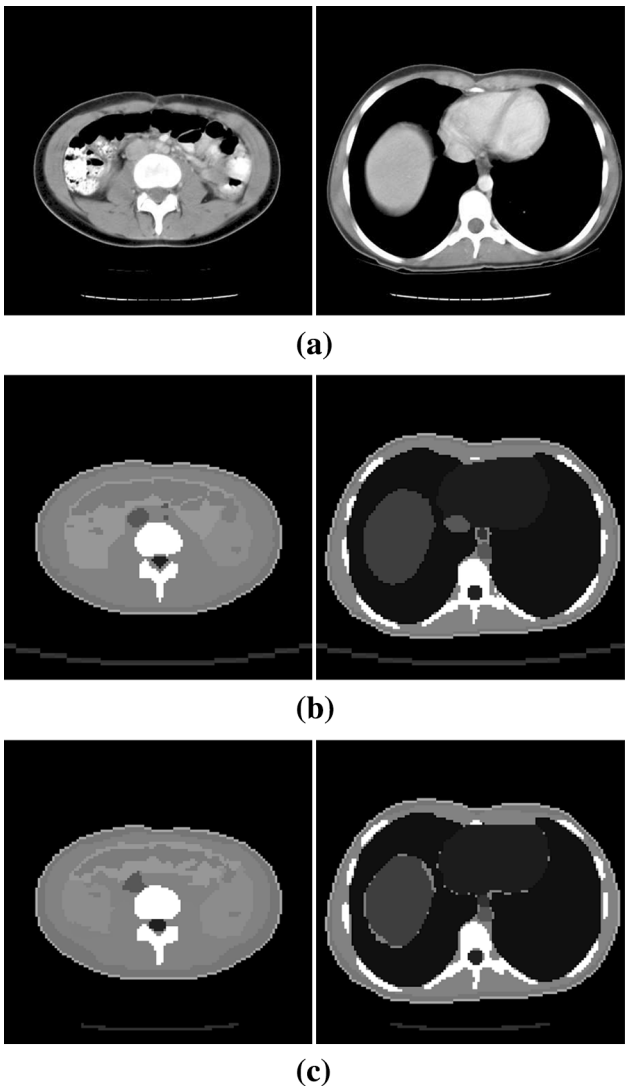

Fig. 4 CT images 68 (*left*) and 48 (*right*) from the ADELAIDE data set: **a** an original 451 × 451 image, **b** as a 200 × 200 image after manual segmentation (cropped back to 128 × 126), **c** as a 128 × 126 image after SRM–GUI segmentation

percentage differences are strongly influenced by the anatomical judgement of the person doing the segmentation.

Discussion

It is to be expected that two independent segmentations of the same data will result in different numbers of voxels being assigned to any given tissue. It is also required for accurate segmentations, that the differences will be small. For eight of the 21 tissues in Table 1, the differences are 10 % or less, while for 13, the voxel numbers are within 18 %. For seven of the 21 tissues the differences are greater than 25 %. They are small organs that are not easily pre-segmented by SRM unless there is good contrast between them and surrounding tissue. In the case of these tissues, relying less on SRM and more on manual techniques for their segmentation would improve the outcome. However for this work we were willing to accept a speedy but possibly less than optimal segmentation for some tissues, if the resulting anatomical model produced credible absorbed doses.

Combining pre-segmentation of images using the statistical region merging technique, with a rapid means of amalgamating regions via a graphical user interface has allowed us to segment CT images in a much shorter time than is possible using manual techniques and standard image-processing software. If the organ doses that result from using the SRM–GUI version of ADELAIDE are close to those achieved using the manually segmented version of ADELAIDE, then the rapid segmentation technique is acceptable for use. From the literature, it may be concluded that organ doses differences as high as $30 * \cong$ when different (but similar in size) computational models are used might be expected. For example: Zhang et al. [30] compared organ doses calculated using two different but similar-sized reference computational models (that they called XCAT and ICRP110) derived from medical images. For an abdomen CT examination of the female models, the average difference for the "partially exposed radiosensitive organs" (marrow, colon, lung, skin, bones) was $14 * \cong$. For the fully irradiated organs (stomach and liver) the average difference was $21 * \cong$. The corresponding values for average organ dose difference when SRM–GUI segmentation is compared to manual segmentation for ADELAIDE are: 11 and 16 %. While not calculating organ doses, Schlattl et al. [31] compared the organ dose conversion coefficients normalized to $CTDI_{vol}$ calculated using the same ICRP110 female phantom used by Zhang et al. [31] (which they refer to as ACP-RF), and their female model "Irene" (they are both 163 cm in height). For a CT slice centered on the stomach, the average difference between ACP-RF and Irene (for adrenals, stomach, liver, gall bladder, spleen, pancreas and kidneys) was 27 %. Since for 17 of the 21 tissues segmented, the MC calculated absorbed doses to the SRM–GUI segmented version are within 18 % of the MC calculated absorbed doses to a manually segmented version of the same anatomy, we conclude that the resulting anatomical voxel model is useful for CT dosimetry. The organ doses to the SRM–GUI segmented version of ADELAIDE are higher for 16 of the 21 values in Table 1. This might be attributed to the fewer voxels of muscle and soft tissue and of skin, and the greater number of voxels segmented to sub-cutaneous fat in the SRM–GUI segmentation (see Table 2). This would provide less shielding to the internal organs.

It is likely that if more time is spent with the GUI to segment tissue whose pixels are difficult to characterise as

Table 2 The number of voxels segmented to each tissue by manual segmentation and by SRM–GUI segmentation

Organ/tissue	Number of voxels by manual seg.	Number of voxels by SRM–GUI seg.	Percentage difference (GUI/manual)
Bone	26,135	41,485	
		Including bone surf	
Bone surface	14,841	na	
Combined bone and bone surface	40,976	41,485	1
Heart	10,689	11,070	4
Spinal cord	1,040	1,308	26
Skin	16,682	15,304	−8
Sub cut fat	42,252	48,864	16
Muscle	139,354	110,537	
	Including soft tissue		
Soft tissue	na	15,365	
Combined muscle and soft tissue	139,354	125,902	−10
Breasts	4,611	4,303	−7
Lungs	65,421	65,726	0.5
Oesophagus	466	548	18
Kidneys	5,419	5,302	−2
Liver	22,696	22,801	0.5
Spleen	3,004	2,702	−10
Stomach	5,086	4,390	−14
Gas in bowel	15,981	14,515	−9
Small bowel	19,184	9,355	
(wall and contents)	Including tra+asc colon		
Large bowel	6,817	22,224	
	des+rec	asc+tra+des+rec	
Combined small and large bowel {including gas}	26,001, {41,982}	31,579, {46,094}	21, {10}
Pancreas	873	511	−42
Gall bladder	125	268	214
Uterus	541	399	−26
Ovaries	162	90	−44
Bladder	282	445	56
Thymus	228	356	56
Trachea	143	315	220
Thyroid	270	159	−41

regions using the SRM technique (such as thymus and trachea), then the differences between the absorbed dose to these tissues in the differently segmented versions of ADELAIDE would decrease. However we were interested in whether a rapidly segmented voxel model would produce accurate absorbed doses so chose not to expend a lot of time using the GUI to finesse the segmentation, choosing instead to minimise segmentation time. While we could not directly compare the segmentation time required by the two techniques—the original manual segmentation of ADELAIDE was spread over about 18 months (not full-time) and the segmentation was often reworked to improve the outcome—SRM–GUI segmentation of the 54 CT images in the ADELAIDE dataset was achieved in 10 working days (about 60 h).

Medical CT images have been used as the source of anatomical data from which to build anatomical models because of the high degree of realism that can be achieved. Skilful manual or semi-automatic segmentation of CT images is time-consuming, but results in organ and tissue boundaries that are smooth and organ sizes, shapes and positions that are anatomically accurate. Except for the smallest tissues, SRM–GUI segmentation can achieve segmentation of comparable accuracy and realism to that of

manual segmentation (compare Fig. 4b, c for the same slice). For the smallest organs or tissues, manual intervention is required. SRM–GUI segmentation probably will not achieve organ boundaries that are as smooth as those that can be achieved manually—even after applying smoothing. However, the SRM–GUI segmentation technique, while it sacrifices smoothness of boundaries for speed of segmentation, maintains anatomically accurate organ size, shape and position. The organ doses calculated using the resulting model are comparable to those calculated with a manually or semi-automatically segmented model. Consequently SRM–GUI segmentation is useful for construction of voxel anatomical models from CT images.

The field of view used to acquire the clinical CT images for ADELAIDE was not quite wide enough to include the entire anatomy of the patient. Consequently any muscle, fat and skin beyond 128 pixels laterally is absent from the SRM–GUI segmentation. This means that there are fewer voxels of skin (15,304 compared with 16,682), and of combined soft tissue and muscle (125 902 voxels compared with 139 354 voxels) in the SRM–GUI segmented version of ADELAIDE than in the manually segmented version. Absent muscle and fat tissue that was adjacent to the skin envelope but superficial to muscle was assigned with the GUI, to subcutaneous fat (rather than reconstructing muscle pixels manually). Hence the SRM–GUI segmentation has more fat voxels than the original manual ADELAIDE segmentation (48,864 compared to 42,252). These differences between the two versions of ADELAIDE will affect the Monte Carlo calculated dose to those and other tissues. However, it was deemed that comparing the dose to the SRM–GUI segmented model (despite having truncated anatomy at the shoulders and hips), with that to the manually segmented version (which has complete anatomy), would be a more rigorous test of the ability of the SRM–GUI segmented anatomical model to produce CT dose calculations that are comparable to those produced with the manually segmented original ADELAIDE. To offset the differences, an abdominal CT examination was chosen for simulation as the truncated anatomy is not directly exposed in the X-ray beam.

Images pre-segmented by SRM still require the user to have anatomical knowledge and to perform some manual segmentation with the GUI. For example thin structures such as skin and small structures such as oesophagus, trachea, gall bladder and ovary still need to be handled manually. Structures that may not be easily visible (such as pancreas and adrenal glands) may also need manual techniques to segment. Thus to some extent, the segmentation outcome will depend on the skill of the person doing the segmentation. The ADELAIDE data set was acquired with a now dated CT scanner—it is likely that newer scanners will provide better images for SRM to work with and that modern data sets will have slices at narrower intervals.

Conclusion

The SRM pre-segmentation technique has been combined with an in-house GUI to segment the same data set of CT images that were used to construct ADELAIDE. The SRM–GUI segmented images were used to construct a new version of the ADELAIDE voxel model of anatomy. The Monte Carlo calculated absorbed doses to the organs and tissues of this new model were compared to those calculated using the original manually segmented ADELAIDE voxel model. For 17 of the 21 tissues for which absorbed dose was calculated, the doses to the SRM–GUI version were within 18 % of the doses to the manually segmented version of ADELAIDE. The SRM–GUI segmentation technique is a valid way to reduce the time taken to construct a voxel tomographic model from CT images. The SRM–GUI method is faster than manual or semi-automated methods. The ability to produce a voxel model in a short time (that is, weeks rather than requiring many months) may make it practical, in the near future, to construct a range of paediatric models that span the size range of children.

Acknowledgments This work was funded by a Channel 7 Children's Research Foundation of SA Grant.

References

1. Gibbs SJ, Pujol A et al (1984) Patient risk from interproximal radiography. Oral Surg Oral Med Oral Pathol 58:347–354
2. Veit R, Zankl M et al Tomographic anthropomorphic models. Part i: Construction technique and description of models of an 8 week old baby and a 7 year old child, Neuherberg, GSF-National Research Center for Environment and Health GSF report 3/89
3. Zubal G, Harrell C et al (1994) Computerised three-dimensional segmented human anatomy. Med Phys 21:299–302
4. Dimbylow PJ (1997) FDTD calculations of the whole-body averaged SAR in an anatomically realistic voxel model of the human body from 1 MHz to 1 GHz. Phys Med Biol 42:479–490
5. Jones DG (1997) A realistic anthropomorphic phantom for calculating organ doses arising from external photon irradiation. Radiat Prot Dosim 72(1):21–29
6. Caon M, Bibbo G, Pattison J (1999) An EGS4-ready tomographic computational model of a 14-year-old female torso for calculating organ doses from CT examinations. Phys Med Biol 44(9):2213–2225
7. Xu XG, Chao TC (2000) VIP-MAN: An image based whole-body adult male model constructed from color photographs of the Visible Human Project for multi-particle Monte Carlo calculations. Health Phys 78(5):476–485
8. Zankl M, Wittman A (2001) The adult male voxel model "Golem" segmented from whole-body CT patient data. Radiat Environ Biophys 40:153–162
9. Saito K, Wittmann A et al (2001) Construction of a computed tomographic phantom for a Japanese male adult and dose calculation system. Radiat Environ Biophys 40:69–76
10. Nipper JC, Williams JL et al (2002) Creation of two tomographic voxel models of paediatric patients in the first year of life. Phys Med Biol 47:3143–3164

11. Nagaoka T, Watanabe S et al (2004) Development of realistic high resolution whole-body voxel models of japanese adult male and female of average height and weight, and application of models to radio-frequency electromagnetic-field dosimetry. Phys Med Biol 49:1–15
12. Kramer R, Khoury HJ et al (2004) All about FAX: a female adult voXel phantom for Monte Carlo calculation in radiation protection dosimetry. Phys Med Biol 49:5203–5216
13. Lee C, Williams J, Lee C, Bolch W (2005) The UF series of tomographic computational phantoms of pediatric patients. Med Phys 32(11):3537–3548
14. Zhang B, Ma J et al (2007) CNMAN: a Chinese adult male voxel phantom constructed from colour photographs of a visible anatomical data set. Radiat Prot Dosim 124(2):130–136
15. Yinxiangzi S, Liwen T, Jonghwi J, Xia X (2013) Development of a voxel-based chinese reference female phantom from color photographs for radiation dosimetry applications. Health Phys 105(6):512–521
16. Kim CH, Choi SH et al (2008) HDRK-man: a whole body voxel model based on high-resolution color slice images of a Korean adult male cadaver. Phys Med Biol 53:4093–4106
17. Park JS, Chung MS et al (2006) Visible Korean human: its techniques and applications. Clin Anat 19:216–224
18. Nock R, Nielsen F (2004) Statistical region merging. IEEE Trans Pattern Anal Mach Intell 26(11):1452–1458
19. Bajger M, Lee G, Caon M (2013) 3D segmentation for multi-organs in CT images. Electron Lett Comput Vis Image Anal 12(2):13–27
20. Schindler K, Suter D (2008) Object detection by global contour shape. Pattern Recognit 41(12):3736–3748
21. Celebi ME, Kingravi HA, Lee J, Van Stoecker W, Malters JM, Iyatomi H, Aslandogan YA, Moss R, Marghoob AA (2007) Fast and accurate border detection in dermoscopy images using Statistical Region Merging. In: Pluim JPW, Reinhardt JM (eds.) Proceedings of SPIE: medical imaging, vol 6512, pp 65123V–1
22. Celebi ME, Kingravi HA, Iyatomi H, Aslandogan YA, Van Stoecker W, Moss R, Malters JM, Grichnik JM, Marghoob AA, Rabinovitz H, Menzies SW (2008) Border detection in dermoscopy images using statistical region merging. Skin Res Technol 347–353. doi:10.1111/j1600-0846.2008.00301.x
23. Bajger M, Ma F, Williams S, Bottema M (2010) Mammographic mass detection with statistical region merging, In: Digital image computing: techniques and applications, Proceedings of DICTA 2010, Sydney, Australia, pp 27–32
24. Lee G, Bajger M, Caon M (2012) Multi-organ segmentation of CT images using statistical region merging. In: Biomedical engineering (BioMed 2012): proceedings of the IASTED international conference, Innsbruck, Austria, pp 199–206
25. Bajger M, Lee G, Caon M (2012) Full-body CT segmentation using 3D extension of two graph-based methods: a feasibility study. In: Signal processing, pattern recognition and applications (SPPRA 2012): proceedings of the IASTED international conference, Crete, Greece, pp 43–50
26. Wong A, Scharcanski J (2011) Fisher-Tippett region-merging approach to transrectal ultrasound prostate lesion segmentation. IEEE Trans Inf Technol Biomed 15(6):900–907
27. Comaniciu D, Meer P (2002) Mean shift: a robust approach toward feature space analysis. IEEE Trans Pattern Anal Mach Intell 24:603–619
28. Shi J, Malik J (2000) Normalized cuts and image segmentation. IEEE Trans Pattern Anal Mach Intell 22:888–905
29. Kawrakow I, Mainegra-Hing E et al The EGSnrc code system: Monte Carlo simulation of electron and photon transport, National Research Council of Canada
30. Zhang Y et al (2012) Organ doses, effective doses and risk indicies in adult CT: comparison of four types of reference phantoms across different examination protocols. Med Phys 39(6):3403–3423
31. Schlattl H et al (2010) Dose conversion coefficients fo CT examinations of adults with automatic tube current modulation. Phys Med Biol 55:6243–6261